

Quantum black holes in the horizon quantum mechanics model at the Large Hadron Collider

Douglas M. Gingrich^{*} and Brennan Undseth[†]

Department of Physics, University of Alberta, Edmonton, Alberta T6G 2G7 Canada

 (Received 21 June 2020; accepted 26 October 2020; published 18 November 2020)

Quantum black hole production at the Large Hadron Collider is investigated using the horizon quantum mechanics model. This model has novel implications for how black holes might be observed in collider experiments. Black hole production is predicted to be possible below the Planck scale, thus leading to the intriguing possibility that black holes could be produced even if the Planck scale is slightly above the collider center of mass energy. In addition, the usual anticipated resonance in the black hole mass distribution is significantly widened in this model. For values of the Planck scale above the current lower limits, the shape of the black hole mass distribution is almost independent of the Planck scale and depends more on the number of extra dimensions. These model features suggest the need for alternative search strategies in collider experiments.

DOI: [10.1103/PhysRevD.102.095020](https://doi.org/10.1103/PhysRevD.102.095020)

I. INTRODUCTION

Low-scale gravity provides an interesting possibility for gaining insight into the hierarchy problem. A wide variety of models based on different paradigms [1–3] have been proposed. A speculative, but intriguing, possibility of most models is the production of quantum black holes in hadron colliders [4,5].

The cross section for black hole production is typically chosen to be the classical geometric form $\hat{\sigma} \approx \pi r_g^2$, where r_g is the gravitational radius which is a function of the black hole mass M and depends on the fundamental parameters of the model. In the large extra dimensions paradigm proposed in Refs. [1,2], the model parameters are the higher-dimensional Planck scale M_D and total number of space-time dimensions D . We will consider the case of a tensionless non-rotating spherically symmetric solution for the gravitational radius [6].

In proton-proton collisions, only a fraction of the total center of mass energy \sqrt{s} is available in the hard-scattering process. We define $s_{x_a x_b} \equiv s\tau \equiv \hat{s}$, where x_a and x_b are the fractional energies of the two colliding partons (assumed massless) relative to the proton energies. The full particle-

level cross section σ is obtained from the parton-level cross section $\hat{\sigma}$ by using [7]

$$\sigma_{pp \rightarrow \text{BH}+X}(s) = \sum_{a,b} \int_{M^2/s}^1 d\tau \int_{\tau}^1 \frac{dx}{x} f_a\left(\frac{\tau}{x}\right) f_b(x) \times \Theta(M - M_{\text{th}}) \hat{\sigma}_{ab \rightarrow \text{BH}}(\hat{s} = M^2), \quad (1)$$

where a and b are the parton types in the two protons, and f_a and f_b are parton distribution functions (PDFs) for the proton. The sum is over all possible quark and gluon pairings. While several prefactors to the cross section have been suggested (see Ref. [7] for a summary) they are not important for this study and will not be considered.

The usual ansatz is that black holes cannot be produced with M below some minimum mass threshold M_{th} . This is emphasized by the use of the Heaviside step function Θ in Eq. (1). The value of M_{th} is typically taken to be M_D for quantum black holes or a few times M_D for classical black holes. Unfortunately, results depend on the subjective choice of the M_{th} cutoff.

A modification to the typical model of black hole formation in hadron colliders is made by the horizon quantum mechanics (HQM) model [8,9]. The wave function for a localized massive particle (source) is taken to be a spherically symmetric Gaussian wave packet in $(D-1)$ spatial dimensions of width ℓ . It is postulated that the form of the wave packet in momentum space is also a Gaussian with width $\Delta = \hbar/\ell$. The simplest case for black hole formation is considered; a D -dimensional Schwarzschild metric and its classical horizon of radius $R_D(M)$. The relativistic mass-shell relation in flat space $E^2 = p^2 + m^2$ is assumed, where the energy E of the particle is expressed

^{*}Also at TRIUMF, Vancouver, BC V6T 2A3 Canada; gingrich@ualberta.ca

[†]Present address: Delft University of Technology, Netherlands; brennan.undseth@gmail.com

Published by the American Physical Society under the terms of the Creative Commons Attribution 4.0 International license. Further distribution of this work must maintain attribution to the author(s) and the published article's title, journal citation, and DOI. Funded by SCOAP³.

in terms of the horizon radius $r_H = R_D(E)$ and m is the rest mass of the source. The momentum-space wave function can then be written in terms of the horizon radius and normalized to give the horizon wave function $\psi_H(r_H)$. The horizon wave function is used to calculate the probability $P_S(r < r_H)$ that the particle is inside a $(D-1)$ -ball of radius r_H and the probability density $\mathcal{P}_H(r_H)$ that the radius of the horizon equals r_H . In this case, the black hole probability depends on the Gaussian width ℓ , particle mass m , and number of spatial dimensions D . It is further assumed that $\ell = M_D \ell_D / m$ is the Compton wavelength of the source, which represents the minimum uncertainty in its size, so that $\Delta = m$, and the probability only depends on m and the number of dimensions D . The system exhibits properties of a black hole when the source is located within the quantized horizon, with the probability of the system being a black hole given by

$$P_{\text{BH}} = \int_0^\infty P_S(r < r_H) \mathcal{P}_H(r_H) dr_H. \quad (2)$$

Explicit expressions of these probabilities are given in Refs. [8,9]. Qualitatively, the use of the HQM probability in the calculation of the proton-proton cross section is akin to replacing the step function located at M_{th} with a sigmoid-like function that varies with M/M_D and depends on D .

The ingredients that go into deriving Eq. (2) are not free of assumptions. In addition, using standard quantum mechanics in the strong gravity regime is ill defined and the formalism is not free of problems. The idea of improving the geometrical cross section by a smoothed step function is not new [10]. Using guiding physical principles similar results to Eq. (2) can be obtained on empirical grounds [10].

The common phenomenology of semiclassical microscopic black holes is not important in this work. Such objects have significant entropy and Hawking evaporate. The evaporation process occurs when the mass of the black hole is well above the Planck scale and thus not close to where HQM effects are important. We thus consider, so called, quantum black holes (QBH), where the object has an event horizon but negligible entropy, and behaves more like a particle in its decay to a few-body—two in our case—final state. Such objects by definition have mass close to the Planck scale and are significantly affected by the HQM model.

The purpose of the work presented here is to evaluate the impact of the HQM model on the production of quantum black holes with emphasis on the signatures for experiments at the Large Hadron Collider (LHC). We begin with a brief description of Monte Carlo (MC) event generation in the HQM model, with more details of the implementation described in the Appendix. We discuss the effects of HQM on the total proton-proton cross section and the differential proton-proton cross section as a function of M . The

possibility of quantum black hole detection in the HQM model in LHC experiments is discussed. A previous publication [11] on this topic made use of ATLAS and CMS results from about 20 fb^{-1} of data at $\sqrt{s} = 8 \text{ TeV}$.

We make use of the following conventions. When comparing models, the QBH model refers to the quantum black hole model with Heaviside step function turn-on typically used by ATLAS and CMS searches at \sqrt{s} of 7 TeV [12–14], 8 TeV [15–20], and 13 TeV [21–28] that does not include any HQM effects. The HQM model will be the model with horizon quantum mechanics effects included. The only difference between these two models is their production turn-on behavior in M/M_D for different D . The total number of space-time dimensions $D = n + 4$, where n is the number of extra dimensions.

II. BLACK HOLE PRODUCTION PROBABILITY

For the purpose of cross section calculations along with event generation, the QBH 3.00 MC quantum black hole event generator [29] is used [30]. In this model [31–33], we consider tensionless nonrotating black holes. The generator only allows for dominant two-body decay of the QBH states. The leading-order CTEQ6L1 [34] PDF set is used for the hard-scattering process. Considering only two-body decays and using the CTEQ6L1 PDF set are consistent with the ATLAS and CMS experiment’s QBH searches. The default settings in QBH are used and the proton-proton center of mass energy is set to 13 TeV. The only parameters that are varied are M_D and D . Cross section calculations in QBH are independent of the number of events generated. For kinematic distributions, 21000 events were generated for each (D, M_D) pair. We work at the parton level and do not hadronize the partons or decay the final state particles; a hadron is considered as a single jet. No energy-momentum

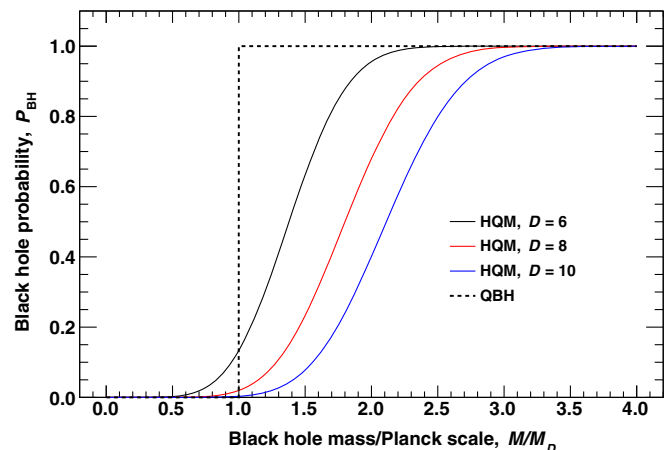


FIG. 1. Horizon quantum mechanics (HQM) probability curves P_{BH} versus black hole mass M relative to the Planck scale M_D for selected total number of space-time dimensions D . The dashed black line represents the step function used in quantum black hole (QBH) models.

TABLE I. Ratio of black hole mass M to Planck scale M_D at $P_{\text{BH}} = 0.5$ for different total number of space-time dimensions D in the horizon quantum mechanics model.

D	6	7	8	9	10	11
M/M_D	1.4	1.6	1.8	2.0	2.1	2.2

smearing or detector simulation has been performed. HQM effects are added to the proton-proton cross section by including the factor P_{BH} of Eq. (2) into Eq. (1):

$$\sigma_{pp \rightarrow \text{BH}+X}(s) = \sum_{a,b} \int_{M^2/s}^1 d\tau \int_{\tau}^1 \frac{dx}{x} f_a\left(\frac{\tau}{x}\right) f_b(x) \times P_{\text{BH}}(M) \hat{\sigma}_{\text{ab} \rightarrow \text{BH}}(\hat{s} = M^2), \quad (3)$$

where P_{BH} requires another numerical integration. The cross section formula is now independent of M_{th} and the model has one less free parameter.

In order to visualize how the HQM probability varies with M, M_D , and D , we have computed the integral in Eq. (2) explicitly, as shown in Fig. 1.

The probability curves suggest some interesting phenomena that are not seen in the QBH model. First, instead of a step function at $M = M_D$, the new curves are smooth. The most notable consequence is that there is a finite probability that a black hole can be formed with $M < M_D$. Second, we see that the probability for a black hole to be produced near M_D is suppressed for high D . In other words, one generally expects more black holes to be produced for low D . This is at odds with the usual effect of dimensionality in the QBH model, where greater D corresponds to a greater geometric cross section. A third observation is that most of the curve is significantly above the value of $M/M_D = 1$. And lastly, the slope in the curves at $P_{\text{BH}} = 0.5$ is not particularly steep.

We can roughly quantify the extent to which the P_{BH} curves create a threshold in the M distribution by considering the midpoint of each curve as the point where $P_{\text{BH}} = 0.5$. These values are shown in Table I. For $D = 6$, the black hole mass threshold rises to slightly above the usual M_D threshold in the QBH model. For $D = 10$, the threshold is more than twice M_D . This means that more dimensions will cause heavy suppression of black hole production in the HQM model, unlike the QBH model in which more black holes will be produced at higher D . The actual values in Table I are model dependent but the trends are indicative.

III. PROTON-PROTON TOTAL CROSS SECTION

We start by analyzing how the inclusion of HQM impacts the proton-proton total cross section as a function of M_D and D . There are two competing factors at play. On one hand, we are multiplying the parton-level cross section by a factor between 0 and 1, which in general decreases the

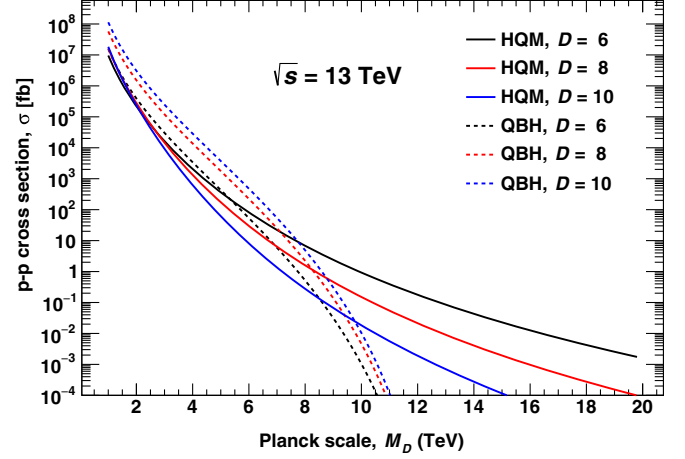


FIG. 2. Proton-proton total cross section σ versus Planck scale M_D at a center of mass energy of 13 TeV. Curves for different models and total number of space-time dimensions D are shown. Solid curves are used for the horizon quantum mechanics (HQM) model and dashed curves are used for the quantum black hole (QBH) model.

cross section. On the other hand, we are considering a wider range of possible M than in the QBH model. In addition, while it is unreasonable to think of producing events in the QBH model if $M_D > \sqrt{s}$, the smooth cutoff imposed by HQM allows for black holes when M_D is above the collider energy. The phenomena are shown in Fig. 2.

The inclusion of HQM suppresses the total cross section for low M_D but predicts a higher cross section than the QBH model at high M_D . It is also interesting to note how the role of dimensionality is reversed in the two models. For a

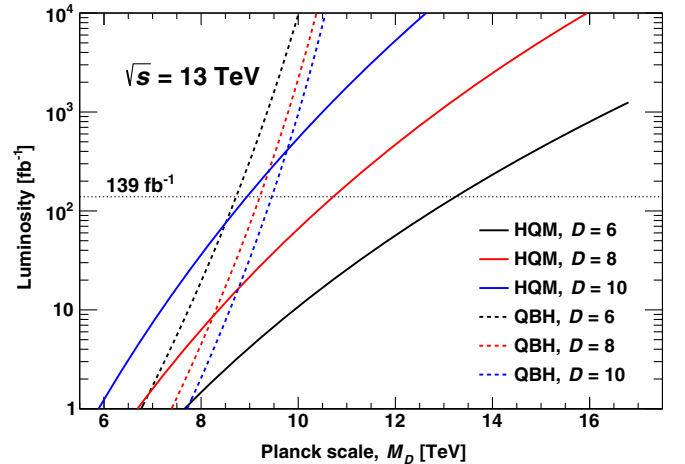


FIG. 3. Luminosity required to produce ten black hole events as a function of Planck scale M_D at a center of mass energy of 13 TeV. Curves for different models and total number of space-time dimensions D are shown. Solid curves are used for the horizon quantum mechanics (HQM) model and dashed curves are used for the quantum black hole (QBH) model. The horizontal dotted line represents a luminosity of 139 fb^{-1} .

given M_D , higher cross sections occur at lower D in the HQM model, except for a small region below about 2 TeV. Also, in the HQM model the cross section at a given M_D is significantly different for different D as M_D increases. Thus over most of the M_D range, dimensionality is significantly more important in the HQM model.

It is also useful to determine the M_D value at which the HQM model cross section crosses over the QBH model cross section, and thus where the HQM model might become more significant. For $D = 6$, $D = 8$, and $D = 10$, the crossovers in M_D occur at approximately 5.4 TeV, 8.2 TeV, and 9.7 TeV, respectively. To understand which region of M_D is interesting, we consider the current lower-limits, at the 95% confidence level, on M_D of 9.9 TeV, 6.3 TeV, and 5.3 TeV for $D = 6$, $D = 8$, and $D = 10$, respectively, set by the CMS [35] and ATLAS [36] experiments. At these M_D limits, black hole production in the HQM model is still well below the QBH model except for $D = 6$ where the HQM model predicts a cross section

of about three orders of magnitude higher than the QBH model.

The lower limits on M_D are based on graviton searches in the same large extra dimensions paradigm [1,2] as used for black hole models, and we thus take them to be applicable to both the QBH and HQM models considered here. Searches for QBHs have set limits on M_{th} (or M_D as a function of M_{th}), and thus do not constrain the HQM model; there are currently no limits on M_D using the HQM model.

The most glaring difference between models occur above the M_D lower limits. While the QBH model cross sections falls sharply as $M_{\text{th}} = M_D$ is pushed toward \sqrt{s} , the HQM model cross sections exhibit a more gradual drop that becomes less steep at higher M_D . This results in some notable properties unique to the HQM model. First, black holes may be produced even if $M_D > \sqrt{s}$. Second, since the cross sections do not converge to zero at $M_D = \sqrt{s}$, dimensionality plays a greater role at high M_D .

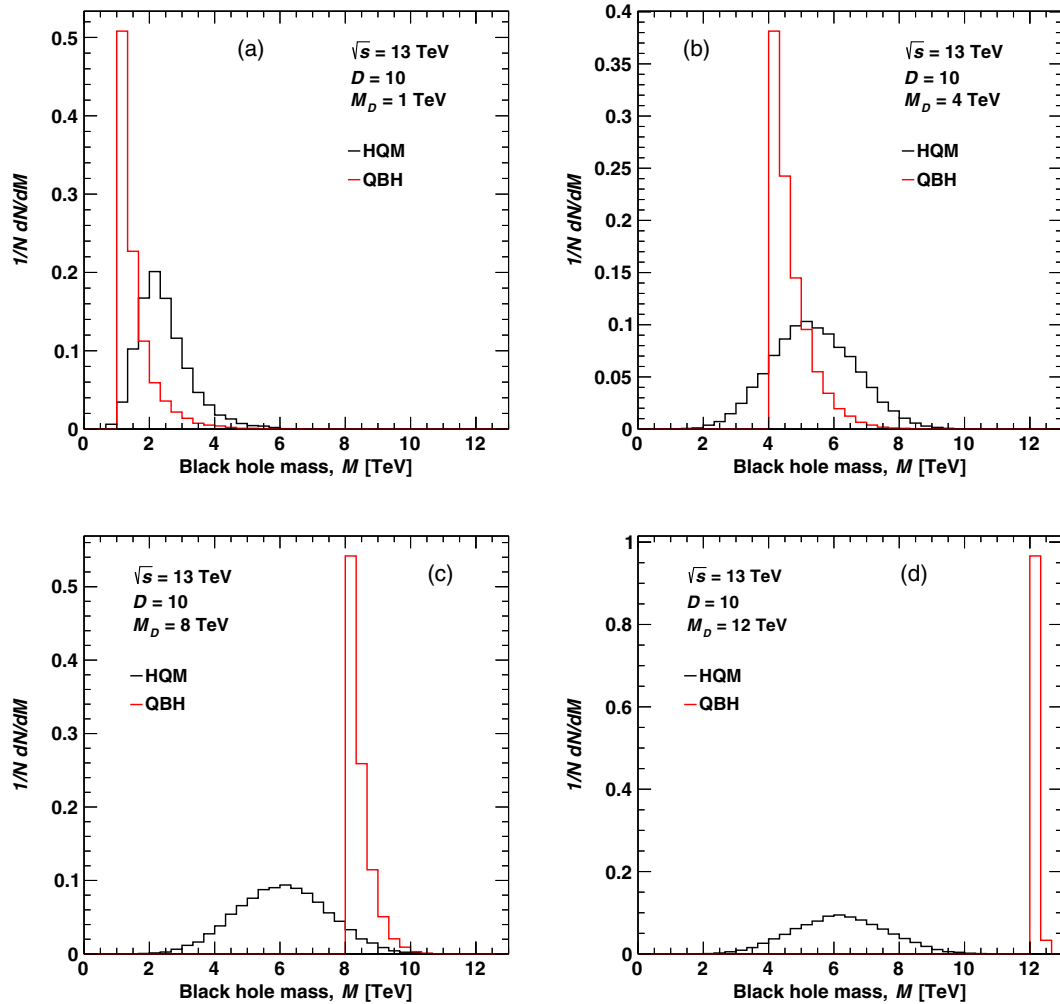


FIG. 4. Quantum black hole (QBH) model and horizon quantum mechanics (HQM) model mass M distributions normalized to unity for (a) $M_D = 1$ TeV, (b) $M_D = 4$ TeV, (c) $M_D = 8$ TeV, and (d) $M_D = 12$ TeV. The center of mass energy is 13 TeV and $D = 10$.

Of particular importance for observing quantum black holes in experiments is the number of black hole events we are able to produce. Typically, a minimum of ten signal events is sought to form a reasonable claim of discovery [37]. In Fig. 3, we plot the luminosity required to produce ten events in proton-proton collisions at $\sqrt{s} = 13$ TeV. Analysis performed by ATLAS and CMS using the full run-2 dataset typically quote a luminosity of about 139 fb^{-1} . Using this luminosity, more than ten events can be produced in the QBH model for M_D less than about 8.7 TeV, 9.2 TeV, and 9.5 TeV for $D = 6$, $D = 8$, and $D = 10$, respectively. The lower limits on M_D would exclude $D = 6$ black holes in the QBH model. The current best lower limit from a direct QBH search is $M_{\text{th}} = M_D > 9.4$ TeV for $D = 10$ [28]. Even with a luminosity of 1 ab^{-1} at $\sqrt{s} = 13$ TeV, the limit on M_{th} in the QBH model is unlikely to go above about 10.5 TeV. Thus, the QBH model is being significantly restricted even at current luminosities.

The LHC is able to produce black holes at much higher values of M_D in the HQM model for most D . At a current luminosity of 139 fb^{-1} , values of M_D in the HQM model are not constrained by the lower limits on M_D , and quantum black holes could exist in the LHC experiment's current datasets. However, as we will see next it will be nontrivial to detect HQM black holes in current ATLAS and CMS datasets even if produced.

IV. PROTON-PROTON DIFFERENTIAL CROSS SECTION

The inclusion of HQM in quantum black hole production has notable implications on the M distribution of black holes. Since the cross sections of QBH and HQM models typically differ by over an order of magnitude (except at very low M_D and near the crossing), it is illustrative to compare the normalized shapes of distributions for M_D of interest. Figure 4 compares M distributions for four selected values of M_D and $D = 10$.

For a small M_D , the HQM model gives the peak structure of the QBH model, but this changes for higher M_D , and M is distributed over a wide range: $2 \lesssim M \lesssim 10$ TeV. This difference in shape is a direct consequence of the shapes of the PDFs and the P_{BH} curve from HQM. The PDFs fall rapidly as parton energies approach $\sqrt{s}/2$. For $M_D = 12$ TeV in the QBH model, a very small cross section is expected since M is limited to the range $12 < M < 13$ TeV. In the $M_D = 12$ TeV HQM model, the lower mass for black holes is dictated by the P_{BH} curve. Black hole masses below 2 TeV are suppressed since $P_{\text{BH}} \approx 0$, and likewise black holes with mass above about 10 TeV are suppressed by the PDFs. This interplay in the HQM model between the convolution of PDFs and P_{BH} gives rise to the shape of the M distributions.

The peak in the QBH M distribution moves up with increasing M_D since the model's definition of M_{th} is a strict cutoff in M . In contrast, the HQM model M distribution

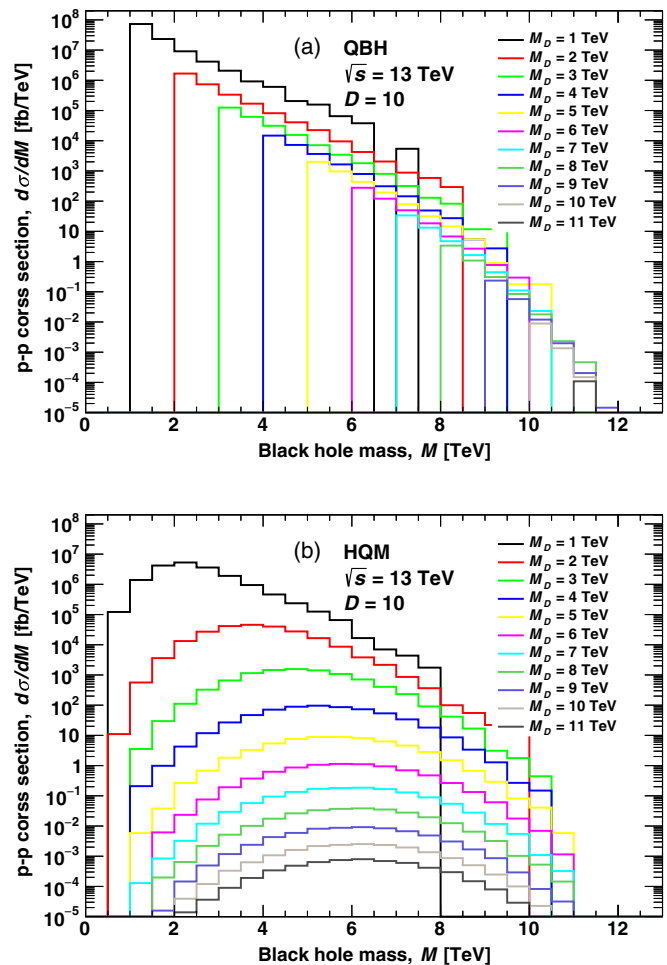


FIG. 5. Quantum black hole (QBH) model (a) and horizon quantum mechanics (HQM) model (b) proton-proton differential cross sections $d\sigma/dM$ versus black hole mass M for selected values of the Planck scale M_D . The center of mass energy is 13 TeV and total number of space-time dimensions $D = 10$.

does not appear to shift up much above $M_D \gtrsim 7$ TeV. This phenomena is explored further in Fig. 5. While the QBH model M distribution moves up with increasing M_D acting as a minimum mass threshold, the HQM model M distributions are much more spread out and the shape of the distributions do not change significantly once M_D exceeds a few TeV. We also observe that in the HQM model it is very difficult to produce black hole masses above ~ 11 TeV, even though M_D is not limited.

The progression of black hole M distributions with M_D in both models is shown in Fig. 6, which plots the mean M as a function of M_D . The QBH model curve gives exactly what is expected, since most black holes are produced with mass M_D , a linear increase in the mean M is observed for all D . This is in contrast to the HQM model which resembles a linear increase only for small M_D and then levels off at a constant mean M for $M_D \gtrsim 8$ TeV. The value of the mean M to which the trend converges is dependent on D . The reason for this is an interplay between the P_{BH}

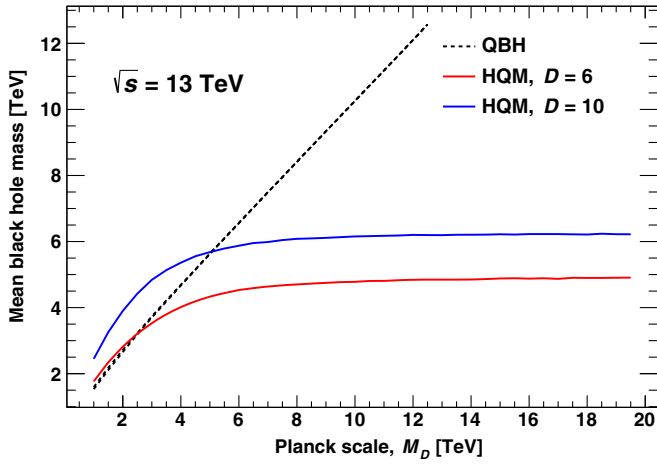


FIG. 6. Mean mass of black hole events as a function of Planck scale M_D at a center of mass energy of 13 TeV. Quantum black hole (QBH) and the horizon quantum mechanics (HQM) models are shown for two values of total number of space-time dimensions D .

curves which approach zero as M approaches zero and the PDFs which approach zero as M approaches \sqrt{s} . The consequence is a “pinching off” that serves to create a mass distribution that does not change shape significantly between the two mass regions where the production of black holes is vanishingly small. The mean M increases with D due to the P_{BH} curve being shifting higher in M/M_D with increasing D , as previously shown in Fig. 1.

Finally, the shape of the HQM model M distribution has implications on how black holes in this model may be detected in the ATLAS and CMS experiments. In the QBH model, black holes are expected to predominantly decay into two-body final states. The majority of these decay products would be quarks and gluons that would hadronize to produce jets. For this reason, ATLAS and CMS have searched for resonances in the mass distribution of dijet events. The branching fraction to dijets is greater than 96% [23]. The experiments have taken the branching fraction to

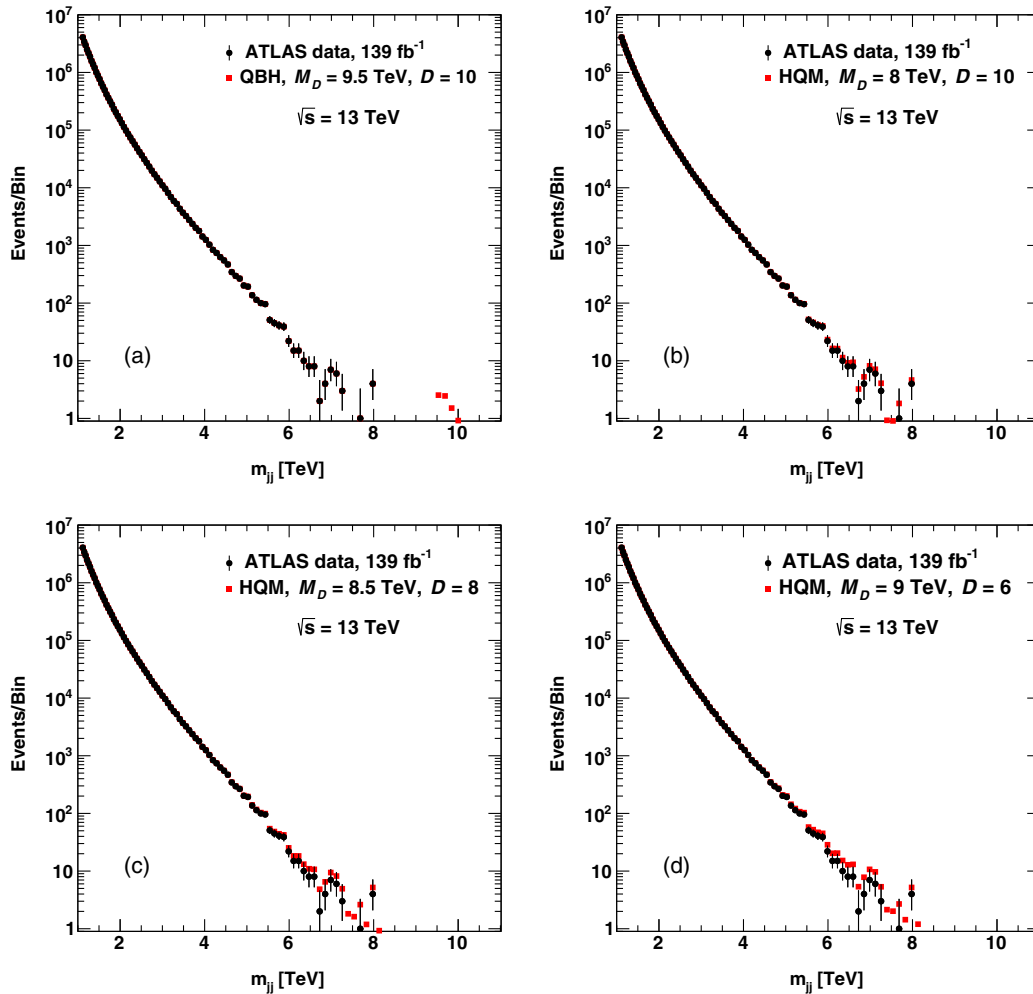


FIG. 7. Black hole dijet mass distributions scaled by cross section to the ATLAS data luminosity and added on top of the ATLAS dijet mass m_{jj} spectrum measured at a center of mass energy of 13 TeV and a luminosity of 139 fb^{-1} [28]. The results are shown for the quantum black hole (QBH) model and horizon quantum mechanics (HQM) model for various values of the Planck scale M_D and the total number of extra space-time dimensions D .

dijets to be unity and have accounted for events with less than two jets in the efficiency. In our study, we have ignored this inefficiency.

To investigate how black holes in the HQM model would appear in these searches, we use 139 fb^{-1} of ATLAS data recorded during run-2 at $\sqrt{s} = 13 \text{ TeV}$ [28,38]. Quantum black hole events are simulated using the same selection criteria, at the particle level, as in the ATLAS analysis. We understand that particle-level selection will only roughly emulate the geometrical acceptance of events in the ATLAS detector, but the signal yields should be indicative of a full experimental analysis [39].

In Fig. 7, the black hole events have been scale by the cross section times luminosity divided by the number of generated events. Fractional events are possible. Figure 7(a) shows an example QBH resonance for $M_D = 9.5 \text{ TeV}$ and $D = 10$. This resonance is beyond the highest dijet mass event obtained by ATLAS. In addition, the decisive lack of such a resonance structure in the dijet mass spectrum has allowed ATLAS to limit black holes in the QBH model to $M_{\text{th}} > 9.4 \text{ TeV}$ for $D = 10$ at the 95% confidence level [28]. Thus, the QBH model in its simplest form is close to being ruled out.

For the HQM model, dijet distributions are shown in Figs. 7(b), 7(c), and 7(d) for $(M_D = 8 \text{ TeV}, D = 10)$, $(M_D = 8.5 \text{ TeV}, D = 8)$, and $(M_D = 9 \text{ TeV}, D = 6)$, respectively. Although ATLAS and CMS have not set limits on the HQM model they have eliminated a wide variety of resonances in the dijet mass spectrum from trigger turn on to about 8 TeV. Thus HQM black hole production resulting in sizable deviations from the smoothly falling dijet mass distribution are not allowed. The values of M_D in the figures have been chosen high enough to not result in a clear enhancement in the dijet mass distribution that ATLAS and CMS have not seen. On the other hand, if the M_D values are chosen higher the number of events becomes insignificant for masses above the ATLAS and CMS data points. It would thus be extremely difficult to observe black holes in the HQM model in the current dijet invariant mass spectrum.

V. DISCOVERY POTENTIAL IN THE DIJET MASS DISTRIBUTION

In order to predict the discovery potential for observing quantum black holes, we take into consideration both the number of events above background and the significance of the signal. For the significance, we use the asymptotic approximation without background uncertainty (see, for example Ref. [40]). The formula comes from using the asymptotic formulas for the distributions of profile likelihood test statistics.

$$\sigma = \sqrt{2 \left[(s+b) \ln \left(1 + \frac{s}{b} \right) - s \right]}, \quad (4)$$

where s is the number of signal events above background and b is the number of background events excluding signal events. The signal events are generated with QBH and the ATLAS background model is taken as the background. We understand that Eq. (4) is an approximation based on a cut-and-count approach, and that one should really include background uncertainties. However, such an analysis is beyond the scope of this work, and is unlikely to change the qualitative findings.

We consider a significant observation to be greater than 5σ . Using a cut-and-count method, significance is calculated by counting events above M_{th} . While this is natural for the QBH model, it is perhaps not so meaningful for the HQM model since many of the events have $M < M_D$. For the sake of comparison, we consider two approaches to calculating the significance for the HQM model. The first is the usual definition, where we consider M_D as a cutoff. In this method M_D values beyond \sqrt{s} cannot be probed. In the second method, we consider all black hole events and count the background from the least massive signal event. We understand that the latter method would be extremely difficult, and probably not even desirable, to realize in an experiment's analysis, but it might be more indicative of a shape-fit procedure that might likely be used.

The event count and significance are presented in Figs. 8 and 9, respectively. While counting HQM model events over the entire mass range gives the greater number of events, the method of counting HQM model events only above M_D give better significances. This could have been anticipated given the large number of background events at low dijet masses. Using either approach to calculating the significance, the discovery potential at allowed values M_D is less for the HQM model than the QBH model. Since the

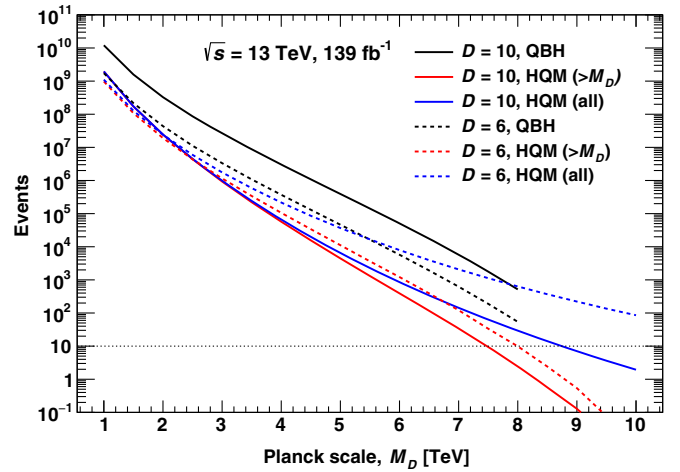


FIG. 8. Predicted number of black hole events versus Planck scale M_D for a center of mass energy of 13 TeV and luminosity of 139 fb^{-1} when selecting events at the parton level according to the same criteria as the search in Ref. [28]. The solid curves are for total space-time dimension $D = 10$ and the dashed curves for $D = 6$.

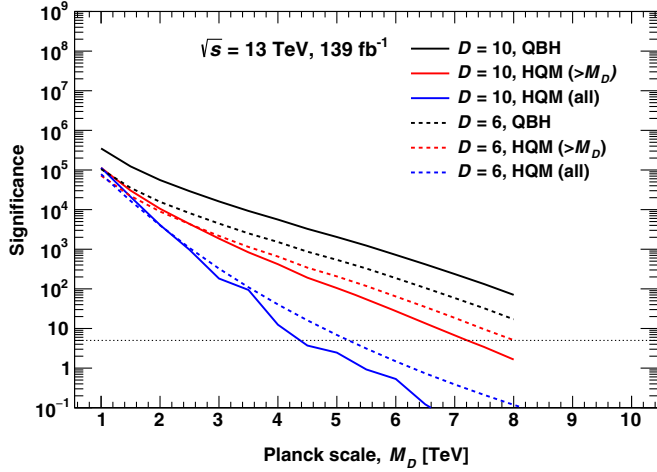


FIG. 9. Significance of a black hole observation above dijet background versus Planck scale M_D for a center of mass energy of 13 TeV and luminosity of 139 fb^{-1} . Events were selected at the parton level according to the same criteria as the search in Ref. [28]. The solid curves are for total space-time dimension $D = 10$ and the dashed curves for $D = 6$.

ATLAS background that we are using does not extend beyond 8.1 TeV, and because of the simple significance formula Eq. (4), the significance curves in Fig. 9 end at $M_D = 8 \text{ TeV}$.

Using the $M > M_D$ counting method and by noting the minimum M_D value given by the ten event and 5σ criteria, we assess the possibility of detecting HQM black holes in ATLAS and CMS. For $D = 10$, the number of signal events is greater than ten for $M_D \lesssim 7.5 \text{ TeV}$. The corresponding significance is greater than 5σ for $M_D \lesssim 7.4 \text{ TeV}$, and this sets the upper limit on M_D to observe black holes in the HQM model. For the $D = 6$ case, greater than ten events occurs when $M_D \lesssim 8.0 \text{ TeV}$ and the significance is greater than 5σ at $M_D \lesssim 8.0 \text{ TeV}$. However, with only one background event, the significance as defined in Eq. (4) slightly overestimates the true significance. In any case, the lower limit on M_D from the CMS experiment [35] for $D = 6$ is 9.9 TeV at the 95% confidence level, thus eliminating the HQM model for $D = 6$.

Given the increase in luminosity and \sqrt{s} in subsequent LHC runs, these discovery potentials stand to increase somewhat. With this thought in mind, we make some predictions at $\sqrt{s} = 13 \text{ TeV}$ on the luminosity required at a given M_D for a meaningful discovery. We assume that the number of background events, based on the background model from Ref. [28], scales linearly with luminosity. When calculating the significance using $M > M_D$ as a cutoff in the cut-and-count method, we have made the additional assumption that event-count is the limiting factor for $M_D > 8 \text{ TeV}$ as this is the highest dijet mass at which the ATLAS background estimate is given. The results are shown in Fig. 10 where we only consider luminosities above 139 fb^{-1} . The luminosity axis of the plot extends out

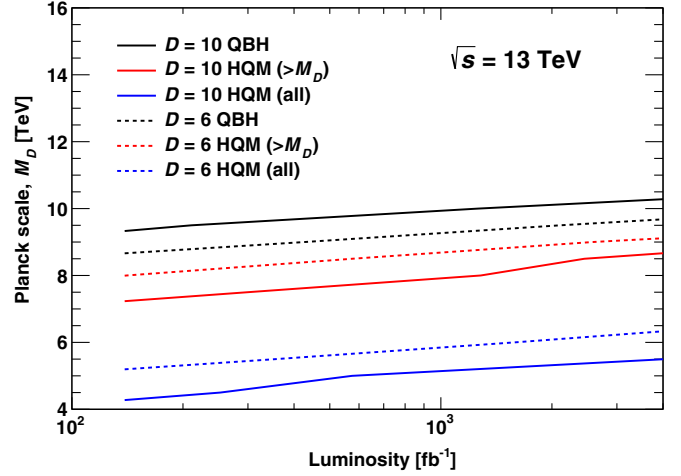


FIG. 10. Minimum luminosity required to produced at least ten signal events and a significance of 5σ at a center of mass energy of 13 TeV. The solid curves are for total space-time dimension $D = 10$ and the dashed curves for $D = 6$.

to 4000 fb^{-1} , inspired by the design integrated luminosity of the High-Luminosity Large Hadron Collider. It is seen that the increase in probing M_D with a reasonable increase in luminosity is not very significant, indicating that we are close to exhausting the search for black holes in both QBH and HQM models using the dijet mass distribution at $\sqrt{s} = 13 \text{ TeV}$. Although we have used a very simplistic approach to estimating the discovery potential, this conclusion is unlikely to change with a more robust estimate.

VI. CONCLUSIONS

Microscopic black hole formation as predicted by HQM was implemented in the QBH MC event generator to investigate the impact on possible black hole production at the LHC. The inclusion of the HQM model serves to decrease the total black hole cross section for small M_D , but the new model is not restricted by a threshold mass requirement. Therefore, HQM predicts black holes may be produced at $M_D \sim \sqrt{s}$. The HQM model is also highly dependent on dimensionality and predicts that a greater number of events may be produced with a smaller D . The M distribution is also greatly affected by HQM with a much wider spread of black hole masses. In other words, there is no resonance structure in the HQM model. This wide M distribution converges to a constant shape for large M_D , which can be considered to be one of the defining features of the HQM model.

The predicted signal in the dijet mass distribution along with the ATLAS run-2 background model were used to estimate the number of signal events and significance. Observations of quantum black holes governed by HQM were predicted to be limited to $M_D \lesssim 8.0 \text{ TeV}$ for $D = 6$ and $M_D \lesssim 7.2 \text{ TeV}$ for $D = 10$.

Given the small potential for observation of HQM black holes in the dijet mass distribution, a discovery in the invariant mass variable is unlikely. Alternatively, an angular search may be performed to distinguish an enhancement of events due to black hole production above QCD background [12,13,21,23,24]. The HQM model does not yet predict any modification to the usual decays in the QBH model; there is no difference between the two models in terms of the shape of angular distributions.

An example angular search could be in the variable χ defined as

$$\chi = e^{|y_1 - y_2|}, \quad (5)$$

where y_1 and y_2 are the rapidities of the two jets. QCD t -channel scattering constituting the background is approximately constant in χ , while s -channel resonances tend to be enhanced at low χ . Because of this, an angular search could help uncover the wide s -channel mass enhancement that is predicted by HQM. Since the predictions of an angular search are highly dependent on the analysis and detector details, we leave it to the ATLAS and CMS collaborations to perform such a search.

Some of the above results were first mentioned in Ref. [11]. Unfortunately, that paper could only make use of ATLAS and CMS results from about 20 fb^{-1} of data at a center of mass energy of 8 TeV. We view our analysis as more comprehensive, benefiting from using recently available experimental data distributions, and up to date.

Lastly, although the HQM model has been used, we do not believe the qualitative results presented here depend specifically on the formula presented in Ref. [9]; similar results would be obtained for any nonsteplike threshold mass production of black holes such as those presented in Ref. [10].

We have implemented and studied a benchmark model and some of the quantitative results are model dependent. It is not our intent to prove or disprove a particular model but to point out the need for alternative search strategies for quantum black holes such as a dijet angular analysis.

ACKNOWLEDGMENTS

We acknowledge the support of the Natural Sciences and Engineering Research Council of Canada (NSERC). Nous remercions le Conseil de recherches en sciences naturelles et en génie du Canada (CRSNG) de son soutien.

APPENDIX: MONTE CARLO EVENT GENERATION

In order to visualize how the HQM probability P_{BH} varies with D , M_D , and M , we computed the integral in Eq. (2) explicitly using numerical integration. As shown in Fig. 1, good accuracy was achieved with the use of Simpson's method and an adequate large number of subdivisions.

A more elegant means of producing the appropriate P_{BH} factor can be performed by MC integration. As a check, we have also produced the curves in Fig. 1 using MC sampling. By integrating and inverting the \mathcal{P}_{H} distribution, random values of the horizon radius r_{H} can be sampled using a uniform distribution of random numbers. Since \mathcal{P}_{H} is a probability density function, using random r_{H} values to calculate P_{S} for a large number of samples effectively computes the expected value for P_{S} (or equivalently, P_{BH}). For completeness, we present this calculation.

We begin from Eq (3.7) in Ref. [9]:

$$\begin{aligned} \mathcal{P}_{\text{H}}(r_{\text{H}}) &= a^{\frac{d}{d-2}} \frac{2(d-2)}{\Gamma(s, 1)} \Theta(r_{\text{H}} - R_d) \\ &\times \exp(-a^2 r_{\text{H}}^{2(d-2)}) r_{\text{H}}^{d-1}, \end{aligned} \quad (\text{A1})$$

where in this Appendix we use the notion of Ref. [9] except we take the total number of spatial dimensions to be d . We have define $a = (d-2)/(2m)$ and $s = d/[2(d-2)]$, and used $\Delta = m$ as in Ref [9]; $\Gamma(s, x) = \int_x^\infty t^{s-1} e^{-t} dt$ is the upper incomplete Gamma function. In addition, we are using Planck units since we are only interested in lengths and masses relative to M_D .

By taking the Heaviside step function to be one, the indefinite integral can be computed:

$$\int \mathcal{P}_{\text{H}}(r_{\text{H}}) dr_{\text{H}} = -\frac{\Gamma(s, a^2 r_{\text{H}}^{2(d-2)})}{\Gamma(s, 1)}. \quad (\text{A2})$$

Substituting a lower limit of $R_d = [2m/(d-2)]^{1/(d-2)}$ and upper limit of r_{H} , to allow calculation of the cumulative distribution function, gives

$$\text{CDF}[\mathcal{P}_{\text{H}}(r_{\text{H}})] = 1 - \frac{\Gamma(s, a^2 r_{\text{H}}^{2(d-2)})}{\Gamma(s, 1)}. \quad (\text{A3})$$

If we generate a uniform random real number u in the interval $(0,1)$ [or $1-u$ in the interval $(1,0)$] and set it equal to Eq. (A3), we can solve for r_{H} by inverting the incomplete Gamma function with respect to its second parameter:

$$r_{\text{H}} = R_d [Q^{-1}(s, Q(s, 1)u)]^{\frac{1}{2(d-2)}}. \quad (\text{A4})$$

Note that $Q^{-1}(s, Q(s, x)) = x$, where Q^{-1} is the inverse of the regularized upper incomplete Gamma function $Q(s, x) = \Gamma(s, x)/\Gamma(s)$. There are numerical methods to optimize this inversion.

Upon randomly sampling the horizon radii from Eq. (A4), we return values of $P_{\text{S}}(r < r_{\text{H}})$ as given by Eq. (3.5) in Ref. [9]:

$$P_{\text{S}}(r < r_{\text{H}}) = \frac{\gamma(\frac{d}{2}, m^2 r_{\text{H}}^2)}{\Gamma(\frac{d}{2})}, \quad (\text{A5})$$

where $\gamma(s, x) = \int_0^x t^{s-1} e^{-t} dt$ is the lower incomplete Gamma function.

The above random horizon generation can simply be looped over with an average of all P_S values giving an approximate value for P_{BH} . We easily recreate the same probability curves as in Fig. 1 which used Simpson's method.

Both the MC method and Simpson's method for calculating P_{BH} have been implemented in QBH. Despite both methods producing the same results, there are technical pros and cons of each method. The MC HQM calculation just presented is the default method.

One additional technicality should be mentioned. Since black hole production in the HQM model allows for M less than M_D there is no lower-mass cutoff in the generator. Instead, the P_{BH} curve imposes its own smooth limit as it

becomes arbitrarily small. To sample M via a power transformation of the cross section used to increase efficiency, we choose an arbitrary minimum of 100 GeV since in practice it is exceedingly rare to generate an event with M this low. For example, selecting a 200 GeV minimum has a negligible impact on the results.

We point out that our curves of P_{BH} are identical to the corresponding figure in Ref. [11] within our ability to read values from their figure. Equation (7) in Ref. [11] disagrees with Eq. (3.8) Ref. [9], although the later cites the former. We believe Eq. (7) in Ref. [11] has the inverse power of (m_d/m) and a normalization difference of $(D-2)^2$. If the formula in the paper was actually used to generate the plot, the curves continue to increase above unity with increasing mass and do not represent probability distributions.

-
- [1] N. Arkani-Hamed, S. Dimopoulos, and G. R. Dvali, *Phys. Lett. B* **429**, 263 (1998).
 - [2] I. Antoniadis, N. Arkani-Hamed, S. Dimopoulos, and G. R. Dvali, *Phys. Lett. B* **436**, 257 (1998).
 - [3] L. Randall and R. Sundrum, *Phys. Rev. Lett.* **83**, 3370 (1999).
 - [4] S. B. Giddings and S. D. Thomas, *Phys. Rev. D* **65**, 056010 (2002).
 - [5] S. Dimopoulos and G. L. Landsberg, *Phys. Rev. Lett.* **87**, 161602 (2001).
 - [6] R. C. Myers and M. J. Perry, *Ann. Phys. (N.Y.)* **172**, 304 (1986).
 - [7] D. M. Gingrich, *Int. J. Mod. Phys. A* **21**, 6653 (2006).
 - [8] R. Casadio, *Eur. Phys. J. C* **75**, 160 (2015).
 - [9] R. Casadio, R. T. Cavalcanti, A. Giugno, and J. Mureika, *Phys. Lett. B* **760**, 36 (2016).
 - [10] J. Mureika, P. Nicolini, and E. Spallucci, *Phys. Rev. D* **85**, 106007 (2012).
 - [11] N. Arsene, R. Casadio, and O. Micu, *Eur. Phys. J. C* **76**, 384 (2016).
 - [12] G. Aad *et al.* (ATLAS Collaboration), *New J. Phys.* **13**, 053044 (2011).
 - [13] G. Aad *et al.* (ATLAS Collaboration), *J. High Energy Phys.* **01** (2013) 029.
 - [14] S. Chatrchyan *et al.* (CMS Collaboration), *J. High Energy Phys.* **01** (2013) 013.
 - [15] G. Aad *et al.* (ATLAS Collaboration), *Phys. Lett. B* **728**, 562 (2014).
 - [16] G. Aad *et al.* (ATLAS Collaboration), *Phys. Rev. Lett.* **112**, 091804 (2014).
 - [17] G. Aad *et al.* (ATLAS Collaboration), *Phys. Rev. D* **90**, 052005 (2014).
 - [18] G. Aad *et al.* (ATLAS Collaboration), *Phys. Rev. D* **91**, 052007 (2015).
 - [19] V. Khachatryan *et al.* (CMS Collaboration), *Phys. Rev. D* **91**, 052009 (2015).
 - [20] V. Khachatryan *et al.* (CMS Collaboration), *Eur. Phys. J. C* **76**, 317 (2016).
 - [21] G. Aad *et al.* (ATLAS Collaboration), *Phys. Lett. B* **754**, 302 (2016).
 - [22] M. Aaboud *et al.* (ATLAS Collaboration), *Eur. Phys. J. C* **76**, 541 (2016).
 - [23] M. Aaboud *et al.* (ATLAS Collaboration), *Phys. Rev. D* **96**, 052004 (2017).
 - [24] A. M. Sirunyan *et al.* (CMS Collaboration), *J. High Energy Phys.* **07** (2017) 013.
 - [25] M. Aaboud *et al.* (ATLAS Collaboration), *Eur. Phys. J. C* **78**, 102 (2018).
 - [26] A. M. Sirunyan *et al.* (CMS Collaboration), *J. High Energy Phys.* **04** (2018) 073.
 - [27] M. Aaboud *et al.* (ATLAS Collaboration), *Phys. Rev. D* **98**, 092008 (2018).
 - [28] G. Aad *et al.* (ATLAS Collaboration), *J. High Energy Phys.* **03** (2020) 145.
 - [29] We use QBH to refer to the quantum black hole model and QBH to refer to the quantum black hole generator of the same name.
 - [30] D. M. Gingrich, *Comput. Phys. Commun.* **181**, 1917 (2010).
 - [31] P. Meade and L. Randall, *J. High Energy Phys.* **05** (2008) 003.
 - [32] X. Calmet, W. Gong, and S. D. H. Hsu, *Phys. Lett. B* **668**, 20 (2008).
 - [33] D. M. Gingrich, *J. Phys. G* **37**, 105008 (2010).
 - [34] J. Pumplun, D. R. Stump, J. Huston, H. L. Lai, P. M. Nadolsky, and W. K. Tung, *J. High Energy Phys.* **07** (2002) 012.
 - [35] A. M. Sirunyan *et al.* (CMS Collaboration), *Phys. Rev. D* **97**, 092005 (2018).
 - [36] M. Aaboud *et al.* (ATLAS Collaboration), *J. High Energy Phys.* **01** (2018) 126.
 - [37] At this point, we are assuming a perfect search for black holes.

- [38] The data is taken from the HEPData repository, <https://www.hepdata.net/record/ins1759712>.
- [39] The quantum black holes we consider are only effected by the rapidity requirements; the simulated events pass the transverse momentum, invariant mass, and azimuthal angle requirements.
- [40] G. Cowan, K. Cranmer, E. Gross, and O. Vitells, *Eur. Phys. J. C* **71**, 1554 (2011); **73**, 2501(E) (2013).